arXiv:2112.02328v1 [nucl-th] 4 Dec 2021

Nuclear potentials relevant to the symmetry energy in chiral models

Niu Li[1], Si-Na Wei[2], Wei-Zhou Jiang[1]*
[1] School of Physics, Southeast University, Nanjing 211189, China
[2] School of Physics and Optoelectronics, South China University of Technology, Guangzhou 510640, China

We employ the extended Nambu-Jona-Lasinio, linear-σ models, and the density-dependent model with chiral limits to work out the mean fields and relevant properties of nuclear matter. To have the constraint from the data, we reexamine the Dirac optical potentials and symmetry potential based on the relativistic impulse approximation (RIA). Unlike the extended NJL and the density-dependent models with the chiral limit in terms of the vanishing scalar density, the extended linear-σ model with a sluggish changing scalar field loses the chiral limit at the high density end. The various scalar fields can characterize the different Schrödinger-equivalent potentials and kinetic symmetry energy in the whole density region and the symmetry potential in the intermediate density region. The drop of the scalar field due to the chiral restoration results in a clear rise of the kinetic symmetry energy. The chiral limit in the models gives rise to the softening of the symmetry potential and thereof the symmetry energy at high densities.

I. INTRODUCTION

Besides the development of the various many-body theories based on the boson exchanges in the quantum field theory, e.g., see Ref. [1], the gauge invariance is regarded to be important to construct the model for the strong-interacting systems. However, the zero-mass gauge bosons are required by the gauge invariance, which becomes a puzzle of the Yang-Mills fields when applying to the realistic interacting systems. The success of the Bardeen-Cooper-Schrieffer theory for superconducting electrons [2] brings the enlightenment that the ground state or vacuum of the interacting systems is not necessary to respect the gauge symmetry. The symmetry invariant models can possess charges, the temporal component of the currents, that break the vacuum (the vacuum is not annihilated by the charge). By early 1960's, it comes to a surge of such model constructions. The typical models are the linear-σ [3, 4] and Nambu-Jona-Lasinio (NJL) [5] models where the order parameters for the chiral symmetry are the scalar condensate $<\bar{\psi}\psi>$ or the scalar field σ. In these models, the potentials are characteristic of the field term of the fourth power that ensures a double-well potential, and the chiral parter is the so-called Nambu-Goldstone boson, the pion that is the fundamental and unique boson in the effective field theory [6]. These models provide some clue to the solution of zero-mass puzzle of the Yang-Mills fields. It is interesting to note that Schwinger has the view that the gauge boson does not necessarily have zero mass for the special vacuum [7], and soon later Anderson adds that the gauge boson and Nambu-Golstone boson can cancel each other to leave the finite mass boson only [8]. These are, in fact, the looming prelude for the Higgs mechanism. This, seemly digressive but instead, restates the importance of the vacuum. Since the original linear-σ and NJL models fail to fit nuclear matter saturation, a dozen of extended models have been developed to fit nuclear matter saturation and properties of finite nuclei [9–20]. In addition, the chiral symmetry can also be manifest by virtue of the vector channel in the hidden local symmetry [21]. The example of such a vector manifestation of chiral symmetry is the model based on the Brown-Rho (BR) scaling [22–24]. In this work, we single out three models from these categories to expose the role of the chiral symmetry in the nuclear and symmetry potentials relevant to the symmetry energy.

Recently, the uncertainty of the symmetry energy has been again a hot issue, since the accurate measurement of ^{208}Pb neutron skin thickness (0.283 ± 0.071 fm) through the weak-interaction electron scattering gives a large span of the symmetry energy slope $L = 106 \pm 37$ MeV [25, 26]. At the same time, a large span of the $42 < L < 117$ MeV is deduced from the spectra of charged pions [27]. These results seem to shake off the previous constraints on the symmetry energy. In the past, the globally average of 28 independent analyses of various data has led to the value of $L = 59 \pm 16$ MeV [28]. With inclusion of the lower ranges either extracted from data [29, 30] or obtained from the ab initio results of neutron matter [31], an average of the L values gives a larger range of 58.7 ± 28.1 MeV [32]. The rising uncertainty of the symmetry energy and the inconsistency in different extractions pose the challenge and meantime the opportunity to study the symmetry energy from multiple angles. We aim to seek the possible hint and/or constraint on the symmetry energy by revisiting the ingredients of the symmetry energy in terms of nuclear potentials in the relativistic chiral models that in general exhibit the broken vacuum, associated tightly with the symmetry energy through the scalar potential.

We will be interested in the relativistic impulse approximation (RIA) that combines the Dirac decomposition of scattering amplitudes with the nuclear scalar and vector densities. The direct combination with the scattering data ensures the simplification in the analysis of tangled factors in the strong interaction. It is known that the optical potentials obtained from the RIA can reproduce the analyzing power and spin-rotation parameter in proton-nuclei scatterings successfully [33–35], in stark contrast with the standard nonrelativistic optical models [36, 37]. In the past, the RIA has also

*Corresponding author, wzjiang@seu.edu.cn

been used to study the symmetry potentials [38–41] and in-medium nucleon-nucleon (NN) cross sections [42, 43]. With the help of the RIA, we study in this work the effects of the chiral symmetry on the symmetry potential. The chiral models will be solved in the mean-field approximation, and also present the result with the usual relativistic mean-field (RMF) model for comparison.

The remaining of the paper is organized as follows. In Sec. II, we briefly introduce a few typical chiral models and the RIA. Results and discussions are presented in Sec. III. A brief summary is given in Sec. IV.

II. BRIEF FORMALISM

A. Models with chiral symmetry

The chiral symmetry plays very important roles in the strong interaction systems. In the QCD, the chiral symmetry is cooperated by the gauge symmetry to resolve the axial anomaly and then point to the more fundamental structure of quarks and leptons [44, 45]. The chiral symmetry also seems to be a probe to the composite structure of hadrons, which is manifest in the NJL model. In particular, the chiral phase transition would generally coincide with the color deconfinement [46].

As for nuclear physics with the broken chiral symmetry, our attention is on the order parameter (the nonvanishing vacuum of the scalar field or condenstate) in chiral models that brings the effects on nuclear potentials, as mentioned in the Introduction. In the following, we interpret simply the extended NJL, linear-σ models and the density-dependent model with chiral limits that are used in this work. The extended NJL model includes the additional interaction terms with the scalar-vector, scalar-isovector couplings (G_{SV}, $G_{\rho S}$) to fit the saturation and density dependence of the symmetry energy. Here, the additional terms are given by [20, 43, 47]

$$\mathcal{L}_{int} = \frac{G_{SV}}{2}[(\bar{\psi}\psi)^2 - (\bar{\psi}\gamma_5\tau\psi)^2][(\bar{\psi}\gamma_\mu\psi)^2 + (\bar{\psi}\gamma_\mu\gamma_5\psi)^2] + \frac{G_{\rho S}}{2}[(\bar{\psi}\gamma_\mu\tau\psi)^2 + (\bar{\psi}\gamma_\mu\gamma_5\tau\psi)^2] \times [(\bar{\psi}\psi)^2 - (\bar{\psi}\gamma_5\tau\psi)^2]. \quad (1)$$

The gap equation in the mean-field approximation can be obtained as

$$M^* = m_0 - (G_S + G_{SV}\rho_B^2 + G_{\rho S}\rho_3^2) < \bar{\psi}\psi >, \quad (2)$$

where G_S is the scalar coupling, and m_0 is the bare nucleon mass.

The linear-σ model with additional scalar-vector coupling can have the saturation that leads to a stiff equation of state (EOS) with a very large incompressibility [9]. Among a large collection of extended models, we choose the one with the following potential obtained from the QCD lattice calculation in the strong coupling limit (SCL) [16]

$$V_{SCL}(\sigma) = \frac{1}{2}B_\sigma\sigma^2 - A_\sigma \log\sigma^2 - C_\sigma\sigma, \quad (3)$$

where the coefficients $A_\sigma = f_\pi^2(m_\sigma^2 - m_\pi^2)/4$, $B_\sigma = (m_\sigma^2 + m_\pi^2)/2$, and $C_\sigma = f_\pi m_\pi^2$. The potential is symmetric about the axis $\sigma = 0$ with the minimum of the potential at $\sigma = f_\pi$. The potential in Eq.(3), instead of the original potential in the fourth power of the σ, avoids the bifurcation that leads to chiral collapse at the lower chiral condensate. Note that the similar $\log\sigma^2$ term also appears in a scheme that includes the coupling to the field of the glueball [10].

The density-dependent models with the chiral limit are similar to the simple Walecka model and the density-dependent parameters are based on the BR scaling. The mean-field potential energy is given by [48]

$$\mathcal{V} = \frac{1}{2}m_\omega^{*2}\omega_0^2 + \frac{1}{2}m_\rho^{*2}b_0^2 + \frac{1}{2}m_\sigma^{*2}\sigma^2, \quad (4)$$

where the asterisk on the meson mass denotes the density dependence. The relevant parametrization (SLC and SLCd [23, 24]) respects the chiral limit in terms of the vanishing scalar density and nucleon effective mass at high densities. For usual RMF models, we choose the parametrization Fsugold that contains the nonlinear self-interactions of the σ and ω mesons [49].

B. Relativistic impulse approximation

In the proton-nucleus scattering, the scattering process can be approximately treated as the incident proton scattered by each of the nucleons in the target nucleus by neglecting the impact of the incident particle on the mean fields. The Dirac optical potential in the RIA can be written as [33, 34]:

$$U_{\rm opt} = -\frac{4\pi i p_{\rm lab}}{M}[F_S\rho_S + \gamma^0 F_V\rho_B], \quad (5)$$

where the forward NN elastic scattering amplitudes F_S and F_V are determined directly from the experimental NN phase shifts [50]. The RIA optical potential has been used to reproduce pA elastic scattering with incident energies above 400 MeV [35] successfully. ρ_S and ρ_B are the spatial scalar and vector densities of infinite nuclear matter,

$$\rho_{S,i} = \int_0^{k_{Fi}} \frac{d^3k}{(2\pi)^3}\frac{M^*}{\sqrt{M^{*2}+k^2}},$$
$$\rho_{B,i} = \frac{k_{Fi}^3}{3\pi^2},\ i = n, p. \quad (6)$$

When the density dependent effective mass M^* of nucleons is obtained from nuclear models, the scalar density can be calculated from Eq.(6) directly. The scalar density with various models given in the above can give the distinct difference at high densities, as shown in Fig. 1. This will give rise to subsequent effects on the optical potentials and relevant quantities. The Dirac optical potential can be expressed in terms of scalar and vector optical potentials:

$$U_{\rm opt} = U_S^{\rm tot} + \gamma_0 U_0^{\rm tot},$$
$$U_S^{\rm tot} = U_S + iW_S,\ U_0^{\rm tot} = U_0 + iW_0, \quad (7)$$

where U_S, W_S, U_0 and W_0 are real scalar, imaginary scalar, real vector and imaginary vector optical potentials, respectively.

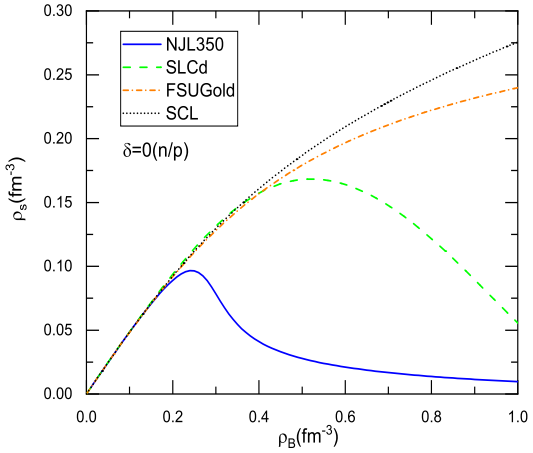


FIG. 1: The scalar density as a function of density in the NJL350, SCL, SLCd, and FSUgold models.

One can derive the Schrödinger-equivalent potential (SEP) from the relativistic dispersion relation as [42]

$$U_{\rm sep}^{\rm tot} = U_S^{\rm tot} + U_0^{\rm tot} + \frac{U_S^{\rm tot\,2} - U_0^{\rm tot\,2}}{2M} + \frac{U_0^{\rm tot} E_{\rm kin}}{M}, \quad (8)$$

where $U_{\rm sep}^{\rm tot} = U_{\rm sep} + iW_{\rm sep}$ and $E_{\rm kin}$ is the nucleon kinetic energy. With the SEP, the symmetry potential is written as

$$U_{\rm sym} = \frac{U_{\rm sep}^n - U_{\rm sep}^p}{2\delta}, \quad (9)$$

with δ being the isospin asymmetry. The $U_{\rm sym}$ is also known as the Lane potential [51].

III. RESULTS AND DISCUSSIONS

The models to be used are the extended NJL model (NJL350) with a momentum cutoff 350 MeV [20, 43, 47], SLCd that is a density-dependent relativistic model with chiral limit [24, 52], the extended linear-σ model in the strong coupling limit (denoted by SCL) [16], and the RMF model FSUgold [49]. The incompressibilities for the models of SCL, NJL350, SLCd, and FSUGold are 279, 262, 230, and 230 MeV, respectively, with corresponding saturation density 0.145, 0.16, 0.16, and 0.145 fm^{-3}.

Figure 2 shows the scalar and vector fields for these models in the mean-field approximation. As shown in Fig. 2, the scalar field with various models can group into two categories: one of which (NJL350 and SLCd) has a fast dropping in the medium, while the other (SCL and FSUGold) has a sluggish decrease. For the chiral models or models with the chiral limit, the scalar field plays a role of the order parameter that reflects the breaking vacuum and probes the chiral restoration in the medium. For the NJL model, the scalar field is, in fact, equivalent to the scalar condensate $< \bar{\psi}\psi >$. A

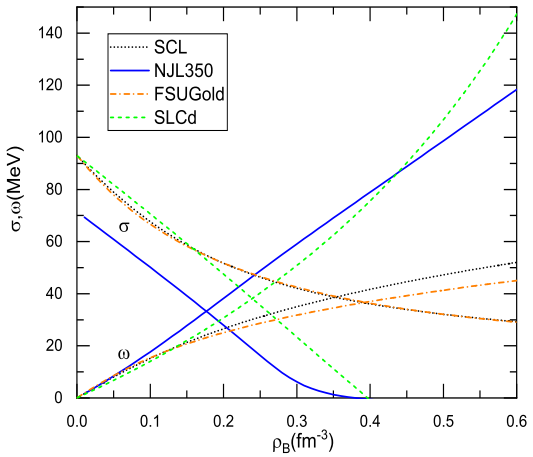


FIG. 2: The scalar and vector fields. The scalar field is redefined for models SLCd and FSUGold as $f_\pi - \sigma$.

clear decrease of the scalar field with the NJL350 and SLCd indicates that these two models have the chiral limit in terms of the vanishing of the scalar field or scalar density (see Fig. 1). The in-medium scalar field with the SCL behaves like that of the RMF model FSUGold, which means that the SCL that respects the chiral symmetry at the vacuum degenerates into a usual RMF model in the medium. As a result, the SCL is not able to restore the chiral symmetry in dense matter even at the sufficiently high density. This is also true for other extended linear-σ models, as it is not able to bring the scalar field down to vanishing in the medium [16]. The slowly varying scalar field also provides considerable attraction that softens the EOS at high density. Together with rather soft vector potential, the SCL and FSUGold are not able to meet the $2M_\odot$ constraint of neutron stars. The situation with the NJL350 and SLCd is quite different by owning the stiff EOS's at high densities and fitting the $2M_\odot$ constraint of neutron stars [20, 48, 53].

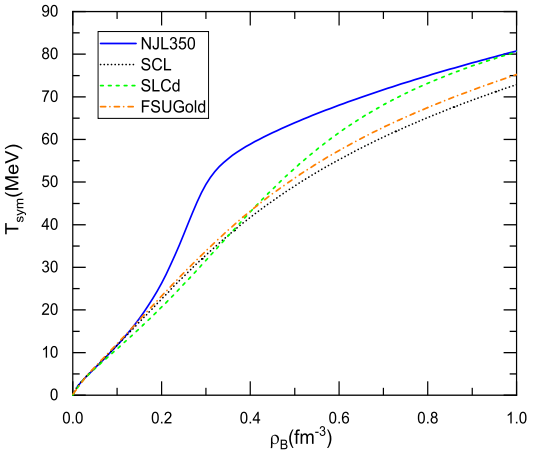


FIG. 3: The kinetic symmetry energy as a function of density with various models.

The scalar field that dictates the nucleon effective mass changes the kinetic symmetry energy (the kinetic

part of the symmetry energy) which in the relativistic formulation is $T_{sym} = k_F^2/6E_F$ with E_F being the Fermi energy. The decreasing nucleon effective mass in dense matter increases the T_{sym} clearly. As shown in Fig. 3, the difference in the kinetic symmetry energy develops beyond saturation density, and it is the most appreciable for the NJL350. With the increase of density, the kinetic symmetry energy with the SLCd comes closer to that with the NJL350 because of the chiral limit of the SLCd. This is a direct evidence that the (partial) restoration of the chiral symmetry has a characteristic contribution to the symmetry energy.

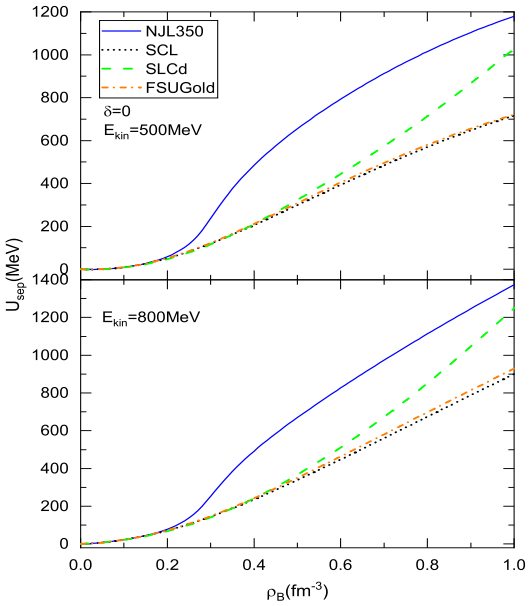


FIG. 4: The SEP as a function of density at the kinetic energy 500 and 800 MeV.

Within the framework of the RIA, the nucleon SEP is derived as in Eq.(8). Figure 4 shows the nucleon SEP of symmetric matter with increasing the density at the two given kinetic energies. The attribution of the difference in various curves is similar to that in Fig. 3 due to the different scalar density. As shown in Fig. 4, the concrete content of the chiral restoration, such as that reflected by the departure in the NJL350 and SLCd, decides the density dependent behavior of the SEP. With the increase of density, the SEP with the SLCd approaches that with NJL350 due to the increasing eclipse of the nucleon mass. For the models SCL and FSUGold that have a sluggish descent of the nucleon mass, the SEP stays away from those with the models that own the chiral limit. Note that the RIA may not work as well at high densities, and the SEP at the high density end would just be referential.

With Eq.(9), we can carry out the symmetry potential as functions of the density or kinetic energy. The symmetry potential is tightly related to the potential part of the symmetry energy [41, 54]. Figure 5 shows the symmetry potential based on various models at $E_{\rm kin} = 500$ and 800 MeV. Since at 800 MeV the RIA results actually include some contributions of the inelastic nucleon-nucleon scattering [43], we focus

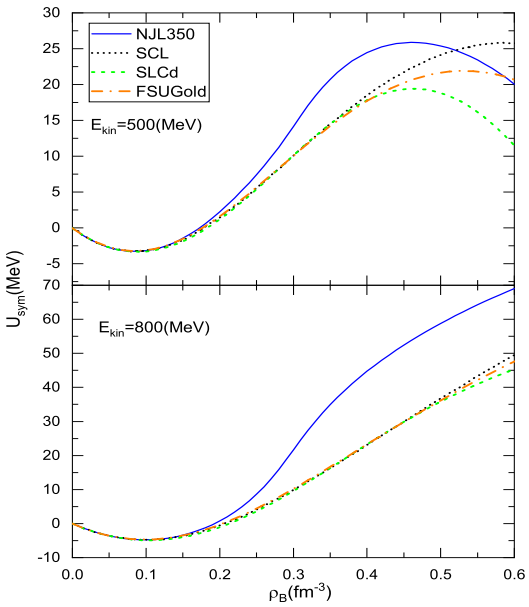


FIG. 5: The symmetry potential as a function of density at kinetic energy $E_{\rm kin} = 500$ and 800 MeV.

mainly on the result at $E_{\rm kin} = 500$ MeV. We see again that the effect of the chiral restoration at the intermediate densities (by the NJL350) gives a very clear rise in the symmetry potential. As shown in the upper panel of Fig. 5, the symmetry potential bends downwards at high densities, which occurs coincidentally in the models NJL350 and SLCd which share the chiral limit. As inferred from Figs. 3 and 5, the symmetry energy appears to be stiffer around saturation density with a larger slope parameter L for the chiral model which owns the chiral limit. It should be pointed out that the symmetry potential at high densities does not follow in a homeomorphic way the difference in the scalar density as those in Figs. 3 and 4. At high densities, there are trespassing between the symmetry potential curves that are subject to the different scalar densities or nucleon effective masses. The reason for this lies in the fact that the variation of the nucleon effective mass against the isospin asymmetry δ can be alternating in various regions of the nucleon effective mass, yielding the disorder in the SEP and symmetry potential for the nonzero isospin asymmetry.

IV. SUMMARY

The chiral symmetry and its breaking define the vacuum and the Goldstone particles, the pion mesons, for the non-perturbative strong interaction system and can add restrictions on the nuclear potentials in the medium. We have revisited the extended NJL and linear-σ models which have a nonzero order parameter, the scalar field or the chiral condensate that plays an important role in the properties of bulk matter. Together with the usual RMF model and the density-dependent model with the chiral limit, we have made a comparative study on the nuclear potentials that are

relevant to the symmetry energy. It is found that the chiral limit in whatever models, chiral or not, ensures a significant reduction of the scalar field and consequently the stiffening of the EOS. Such a stiffening due to the chiral limit is also observed in the Schrödinger-equivalent potentials and the kinetic symmetry energy. In addition, we find that the models with the chiral limit bring the coincident softening of the symmetry potential at high densities, which suggests the softening of the symmetry energy at high densities. On the contrary, the sluggish descent of the scalar field makes the extended linear-σ model to be absent from the chiral limit in the finite density region and accordingly degenerate into the usual RMF model at high densities.

ACKNOWLEDGMENT

The work was supported in part by the National Natural Science Foundation of China under Grant No. 11775049.

[1] R. Brockmann and R. Machleidt, Phys. Rev. C **42**, 1965 (1990).
[2] J. Bardeen, L. N. Cooper, and J.R. Schrieffer, Phys. Rev. **106**, 162 (1957).
[3] J. Schwinger, Ann. Phys. (N.Y.) **2**, 407 (1957).
[4] M. Gell-Mann, M. Lévy, Nuovo Cimento **16**, 705 (1960).
[5] Y. Nambu, G. Jona-Lasinio, Phys. Rev. **122**, 345 (1961).
[6] S. Weinberg, Physica A **96**, 327 (1979).
[7] J. Schwinger, Phys. Rev. **125**, 397 (1962).
[8] P. W. Anderson, Phys. Rev. **130**, 439 (1963).
[9] J. Boguta, Phys. lett. B **120**, 34 (1983).
[10] E. K. Heide, S. Rudaz, and P. J. Ellis, Nucl. Phys. A **571**, 713 (1994).
[11] R. J. Furnstahl and B. D. Serot and H. Tang, Nucl. phys. A **615**, 441 (1997).
[12] P. K. Sahu and A. Ohnishi, Prog. Theor. Phys. **104**, 1163 (2000).
[13] I. Mishustin, Phys. Rep. **391**, 363 (2004).
[14] M. Buballa, Phys. Rep. **407**, 205 (2005).
[15] D. Zschiesche, L. Tolos, J. Schaffner-Bielich, and R. D. Pisarski, Phys. Rev. C **75**,055202 (2007).
[16] K. Tsubakihara and A. Ohnishi, Prog. Theor. Phys. **117**, 903 (2007).
[17] T. K. Jha and H. Mishra, Phys. Rev. C **78**, 065802 (2008).
[18] J. Hu, Y. Ogawa, H. Toki, and A. Hosaka, Phys. Rev. C **79**, 024305 (2009).
[19] S. Janowski, D. Parganlija, F. Giacosa, and D. H. Rischke, Phys. Rev. D, **84**,054007 (2011).
[20] S. N. Wei, W. Z. Jiang, R. Y. Yang, and D. R. Zhang, Phys. Lett. B **763**, 145 (2016).
[21] G. E. Brown, M. Rho, Phys. Rep. **396**, 1 (2004); ibid. **398**,301 (2004).
[22] C. Song, Phys. Rep. **347**, 289 (2001).
[23] W. Z. Jiang, B. A. Li, and L. W. Chen, Phys. Lett. B **653**, 184 (2007).
[24] W. Z. Jiang, B. A. Li, and L. W. Chen, Phys. Rev. C **76**, 054314 (2007).
[25] D. Adhikari, H. Albataineh, D. Androic, K. Anio, et al. Phys. Rev. Lett. **126**, 172502 (2021).
[26] B. T. Reed, F. J. Fattoyev, C. J. Horowitz, and J. Piekarewicz, Phys. Rev. Lett. **126**, 172503 (2021).
[27] J. Estee, W. G. Lynch, C. Y. Tsang, J. Barney, G. Jhang, M. B. Tsang, R. Wang, et al, Phys. Rev. Lett. **126**, 162701 (2021).
[28] B.A. Li and X. Han, Phys. Lett. B **727**, 276 (2013).
[29] J. M. Lattimer and Y. Lim, Astrophys. J. **771**, 51 (2013).
[30] J. M. Lattimer and A. W. Steiner, Eur. Phys. J. A **50**, 40 (2014).
[31] K. Hebeler, J. M. Lattimer, C. J. Pethick, and A. Schwenk, Astrophys. J. **773**, 11, (2013).
[32] M. Oertel, M. Hempel, T. Klähn, and S. Typel, Rev. Mod. Phys. **89**, 015007 (2017).
[33] J. A. McNeil, L. Ray, and S. J. Wallace, Phys. Rev. C **27**, 2123 (1983).
[34] J. A. McNeil, J. R. Shepard, and S. J. Wallace, Phys. Rev. Lett. **50**, 1439 (1983).
[35] L. Ray and G. W. Hoffmann, Phys. Rev. C **31**, 538 (1985).
[36] J. P. Auger, J. Gillespie, and R. J. Lombard, Nucl. Phys. A **212**, 372 (1976).
[37] B. Klem, G. Igo, R. Talaga, et.al., Phys. Bev. Lett. **38**, 1272 (1977).
[38] R. Chen, B. J. Cai, L. W. Chen, B. A. Li, X. H. Li, and C. Xu, Phys. Rev. C **85**, 024305 (2012).
[39] R. Wang, L.W. Chen, and Y. Zhou, Phys. Rev. C **98**, 054618 (2018).
[40] Z. H. Li, L.W. Chen, C. M. Ko, B. A. Li, and H. R. Ma, Phys. Rev. C **74**, 044613 (2006).
[41] L. W. Chen, C. M. Ko, and B. A. Li, Phys. Rev. C **72**, 064606 (2005).
[42] W. Z. Jiang, B. A. Li, and L. W. Chen, Phys. Rev. C **76**, 044604 (2007).
[43] S. N. Wei, R. Y. Yang, J. Ye, N. Li, and W. Z. Jiang, Phys. Rev. C **103**, 064604 (2021).
[44] J.C. Pati, A. Salam, J. Strathdee, Phys. Lett. B **59**, 265 (1975).
[45] K. Huang, Quarks, leptons, and gauge fields, (World Scientific, 1992).
[46] S. Coleman and E. Witten, Phys. Rev. Lett. **45**, 100 (1980).
[47] S. N. Wei, R. Y. Yang, and W. Z. Jiang, Chin. Phys. C **42**, 054103 (2018).
[48] W. Z. Shangguan, Z. Q. Huang, S. N. Wei, and W. Z. Jiang, Phys. Rev. D **104**, 063035 (2021).
[49] B. G. Todd-Rutel and J. Piekarewicz, Phys. Rev. Lett. **95**, 122501 (2005).
[50] R. A. Arndt, L. D. Roper, R. A. Bryan, R. B. Clark, B. J. VerWest, and P. Signell, Phys. Rev.D **28**, 97(1983).
[51] A. M. Lane, Nucl. Phys. **35**, 676 (1962).
[52] W. Z. Jiang, Chin. Phys. C **37**, 064101 (2013).
[53] W. Z. Jiang, B. A. Li, and L. W. Chen, Astrophys. J. **756**, 56 (2012).
[54] C. Xu, B.-A. Li, and L.-W. Chen, Phys. Rev. C **82**, 054607 (2010).